# Connecting molecular simulations and laboratory experiments for the study of time-resolved cation-exchange process in the interlayer of swelling clay minerals

Emmanuel Tertre, Baptiste Dazas, Ali Asaad, Eric Ferrage, Brian Gregoire, Fabien Hubert, Alfred Delville, Frédérick Delay

# Connecting molecular simulations and laboratory experiments for the study of time-resolved cation-exchange process in the interlayer of swelling clay minerals

Emmanuel Tertre[a,*], Baptiste Dazas[a], Ali Asaad[a], Eric Ferrage[a], Brian Gregoire[a], Fabien Hubert[a], Alfred Delville[b], Frederick Delay[c]

[a] Université de Poitiers/CNRS, UMR 7285 IC2MP, Equipe HydrASA, 5 rue Albert Turpain, 86073 Poitiers cedex 9, France.

[b] Université d'Orléans/CNRS, UMR 7374 ICMN, 45071 Orléans, France.

[c] Université de Strasbourg/CNRS, UMR 7517 LHyGeS, 1 rue Blessig, 67000 Strasbourg, France.

[*]Email of the corresponding author:

Emmanuel Tertre (emmanuel.tertre@univ-poitiers.fr)

**Keywords: vermiculite; cation; interlayer of clay mineral; finite-volume model for diffusion; self-diffusion coefficient; up-scaling.**

**Abstract**

In the context of element migration in clay-rich media, self-diffusion coefficients of interlayer cations in swelling clay minerals obtained from molecular simulations are rarely used by macroscopic models predicting cation-exchange processes. Based on experiments and simulations, this study aims at (i) making a connection between molecular and sample scale processes to predict the dynamics of cation-exchange reactions between the interlayer space of millimetre disks of vermiculite and aqueous reservoirs, and (ii) assessing the role played by both self-diffusion and selectivity coefficients on this process.

Time-resolved cation exchange experiments were performed using Ca-saturated vermiculite disks immersed in aqueous reservoirs with different NaCl or $SrCl_2$ salinities. The results were reproduced via a finite-volume model constrained by (i) cation self-diffusion coefficients calculated by molecular dynamics simulations and (ii) interlayer selectivity coefficients drawn from "batch" cation-exchange isotherms.

Results showed that considering the averaged values for both the cation-exchange selectivity coefficients and self-diffusion coefficients of the slowest interlayer cation led to good agreement between the experiments and simulations, validating the modelling strategy for the connection between the molecular and laboratory time scales. A sensitivity test regarding the influence of the two input parameters on the overall results was then performed. This study underlined a constrained upscaling strategy to better assess the role played by different intrinsic parameters of the clay/water systems (molecular self-diffusion coefficients in the interlayer space vs. selectivity coefficient) on the diffusion of cations during cation-exchange reaction in clay-rich media.

## 1. Introduction

Diffusion is the main transport process of water and chemical species in shales and engineered clay-rich barriers considered for the storage of nuclear wastes (see reviews of Bourg et al., 2003 and Charlet et al., 2017 among others). In addition, due to the high compaction of these environments, diffusion in the interlayer spaces of the swelling clay minerals is one of the principal processes controlling the migration of water and cations (Glaus et al., 2007). In this context, numerous models based on a continuum approach coupling diffusion and adsorption/desorption processes are available to describe the reactive transport of cations in compacted clayey porous media (Appelo and Wersin, 2007; Birgersson and Karnland, 2009; Jougnot et al., 2009; Appelo et al., 2010; Tachi and Yotsuji, 2014; Tachi et al., 2014; Tournassat and Steefel, 2015; Tinnacher et al., 2016). Among them, the most exhaustive models (Appelo and Wersin, 2007; Appelo et al., 2010; Tachi and Yotsuji, 2014; Tachi et al., 2014; Tournassat and Steefel, 2015; Tinnacher et al., 2016) account for the reduced mobilities of cations (as compared to bulk water) near the negative surfaces of clay particles (such as interlayer surfaces), as indicated by molecular dynamic simulation studies (Marry and Turcq, 2003; Tournassat et al., 2009; Michot et al., 2012; Tinnacher et al., 2016 among others). These models typically consider a unique pore size value (usually, within the nanometre range) and differ from each other in the way they describe the geometry of the electrical double layer (i.e., presence of the Stern layer or not, in addition to the diffuse ion swarm) and the evolution of the electrical potential from the surface to the nanopore centre. These models present the great advantages, over empirical models (i.e., those based on the Fick's first law) to (i) provide the coupling between transport and chemical processes (i.e., sorption reactions via selectivity coefficients), and (ii) to constrain the diffusion process at the sample scale using mobility determined at the

molecular scale (Tournassat and Steefel, 2019). Applications of these reactive transport codes coupling transport and chemical processes, as Phreeqc® (Parkhurst and Appelo, 2013) or CrunchFlow MC (now CrunchClay ; Steefel et al., 2015), were proved to be extremely efficient at describing the transport of multi-species in complex heterogeneous and charged clay porous materials submitted to various chemical and physical perturbations (e.g., sorption, dissolution/precipitation, change of porosity distribution due to salinity gradient).

However, at the scale of an individual clay particle (i.e., dispersed system), the situation differs for the specific case of time-resolved ion-exchange processes. One study tried to connect molecular and sample scales to predict cation-exchange rates at the interface between the interlayer of swelling clay minerals and aqueous reservoirs (Tertre et al., 2015). This was made possible using millimetre-sized vermiculite disks initially Ca-saturated and immersed in NaCl solutions with different salinities. Vermiculite does not display osmotic swelling, contrary to smectitic clays commonly used in macroscopic diffusion experiments (see Glaus et al., 2007 among others). This sample thus keeps a constant hydration state, allowing to derive self-diffusion coefficients from computational methods such as molecular simulations. By coupling molecular dynamic (MD) simulations at the molecular scale and Brownian dynamic (BD) simulations at the sample scale, authors indicated that the experimental data of the dynamics of the $Na^+$-for-$Ca^{2+}$ ion exchange reaction at the interface between the interlayer of the clay mineral and the bulk reservoir were well reproduced (Tertre et al., 2015). In this previous study, it was also shown that for aqueous reservoirs with high salinities the diffusion during cation-exchange reactions was only driven by the sole self-diffusion coefficients of interlayer cations leading to the generation of interlayer gradients varying with the $Na^+/Ca^{2+}$ interlayer occupancy and diffusion time. Notably, the integration of BD into continuum approaches is difficult, even

though the technique is powerful to assess the influence of the geometry of the porous media on the macroscopic diffusion (Dabat et al., 2020). As an alternative, Tournassat and Steefel (2015) used a model based on continuous equations and properties of negative surfaces to successfully interpret the experimental dataset previously reported in Tertre et al. (2015). However, the interlayer diffusion coefficients of cations reported by Tournassat and Steefel (2015) were found to vary with the salinity of the aqueous reservoir. These molecular diffusion coefficients are thus apparent and cannot be considered as self-diffusion coefficients (i.e., depending only on the environment of the confined probe in the interlayer space at thermodynamic equilibrium) commonly derived from molecular simulations. Accordingly, the question remains open regarding the ability of continuum approaches to connect the molecular self-diffusion coefficients derived from molecular simulations at short timescales with laboratory experiments timescales for cation-exchange reactions in a single clay disk immersed in different aqueous reservoirs.

In this context, the aim of this present work is firstly to assess, within the framework of continuous approaches, the possibility to account for molecular self-diffusion coefficients to predict the dynamics of the cation-exchange reaction in the case of a single disk immersed in aqueous reservoirs. For this purpose a simple finite-volume model constrained by (i) interlayer self-diffusion coefficients stemming from MD simulations and (ii) interlayer selectivity coefficients describing interlayer exchange is used to simulate cation-exchange rates as a function of the diffusion time for a millimetre-sized particle immersed in an aqueous reservoir characterized by different concentrations. Secondly, the roles played by both self-diffusion and selectivity coefficients on the dynamics of the cation-exchange are assessed by the confrontation of predicted data with the experimental dataset. This includes $Sr^{2+}$-for-$Ca^{2+}$ and $Na^{+}$-for-$Ca^{2+}$ ion-exchange data obtained with millimetre vermiculite disks.

Finally, the sensitivity of the proposed model to self-diffusion and selectivity coefficients values used is evaluated, which introduces a discussion on the parameters required to predict the dynamics of the cation-exchange process in diffusion models.

## 2. Experimental method and modelling

### *2.1 Cation-exchange experiments on individual vermiculite disks*

Experiments were performed according to the method detailed in Tertre et al. (2015). Briefly, thin disks of Ca-vermiculite (5 mm in diameter; ≈ 0.6-0.7 mm in thickness), obtained by punching large monocrystal pieces of vermiculite from Santa Olalla (Huelva, Spain), were immersed in aqueous reservoirs of NaCl and $SrCl_2$ at different initial concentrations, and the release of Ca from the disk to the solution was measured with respect to time. The solid/solution ratio used for these experiments is equal to 0.12 $g_{hydrated\text{-}solid}/kg_{water}$ (i.e., typically 30 mg of hydrated solid in 250 mL of aqueous solution), corresponding to $1.05x10^{-4}$ $mol_{Ca}/kg_{water}$ considering a cationic exchange capacity (CEC) of 175 meq/100 $g_{hydrated\text{-}solid}$ in agreement with the value reported for this parameter in the literature (Dzene et al., 2016). Experimental results are expressed in terms of the % Ca (relative to the CEC) released in solution as a function of the diffusion time. Aqueous concentrations of Ca cations were measured using an atomic absorption spectrophotometer (Varian AA240FS) with all samples analyzed in 2% $HNO_3$ solutions. To take into account possible interferences during analyses due to the extreme saline conditions used, $LaCl_3$ and KCl solutions were added in the samples. As recommended by Lajunen and Peramaki (2004), amounts of these added solutions were chosen in order to have final concentrations in the samples equal to 1 and 2 $g/kg_{water}$ for $LaCl_3$ and KCl, respectively. In this present study, $Sr^{2+}$-

for-$Ca^{2+}$ data were obtained for three contrasted initial aqueous $SrCl_2$ concentrations (i.e., $10^{-2}$, $2x10^{-4}$, and $3x10^{-5}$ mol/$kg_{water}$). To increase the number of available experimental data, additional $Na^+$-for-$Ca^{2+}$ data were also collected using NaCl initial concentrations equal to $5x10^{-2}$ and $3x10^{-3}$ mol/$kg_{water}$, completing the $Na^+$-for-$Ca^{2+}$ experimental data set reported in Tertre et al. (2015) for NaCl initial concentrations equal to 1, $5x10^{-2}$ and $3x10^{-3}$ mol/$kg_{water}$. The pH was measured throughout the experiments and was found to be fairly constant at approximately 5.9±0.15. Finally, no change in sample disk integrity (i.e., dissolution) was observed during the experimental timespan.

*2.2 Self-diffusion coefficients obtained by microscopic simulations*

Self-diffusion coefficients of interlayer cations were obtained for different interlayer $Ca^{2+}$/$Sr^{2+}$ and $Ca^{2+}$/$Na^+$ occupancies by MD simulations. These calculations were based on molecular clay configurations derived from Grand Canonical Monte Carlo (GCMC) simulations representative of the hydrated clay mineral used for the experiment. These coefficients will be compared for the purpose of validation in the results and discussion section to data reported in the literature for other hydrated clay structures.

2.2.1 Grand Canonical Monte Carlo (GCMC) simulations

A molecular structure was first obtained by GCMC (Delville, 1991; Allen and Tildesley, 1994). This structure is composed of 3 clay layers, each made of 60 unit cells (i.e., 10 and 6 along the a and b unit-cell parameters, respectively), leading to simulation cells large enough

(53.2 Å x 55.26 Å x 44.76 Å) to study the radial diffusion of confined cations. The chemical composition of the unit cell used for the calculation is:

$$[Si_{5.65}Al_{2.35}Mg_{5.32}Al_{0.58}Fe^{+III}_{0.1}O_{20}(OH)_4](Ca_xSr_yNa_z), XH_2O$$

where $2x + 2y + z = 1.67$, with 1.67 corresponding to the structural charge of the unit cell. It should be noted that the structural formula used was adapted from that proposed in the literature by Argüelles et al. (2010) for a by-hydrated Mg-structure:

$$[Si_{5.66}Al_{2.34}Mg_{4.92}Al_{0.60}Fe^{+II}_{0.44}Ti_{0.04}O_{20}(OH)_4](Mg_{0.76}Ca_{0.06}Na_{0.04}), 7.63H_2O$$

The purpose was to homogenize the number of substituted atoms between the 3 layers as well as counterions while maintaining the overall charge and charge localization. $X$ is the number of confined water molecules per unit cell determined at a prescribed temperature (T = 298 K) and a water chemical potential ($p/p_0$ = 1) representative of water-saturated conditions. This value has been set to 10.0, 10.35 and 9.6 for Ca, Sr and Na by-hydrated end-members, respectively. Finally, note that simulation cells are directly in contact with the periodic boundaries leading then to cells mimicking «infinite» layer.

The thickness of the clay layer used for the calculations was fixed to 14.92 Å, corresponding to the value proposed by de la Calle and Suquet (1988) for a Ca-vermiculite layer immersed in water. This value was used irrespective of the equivalent fraction of $Ca^{2+}$ (i.e., XCa) in the layers during exchange with either $Sr^{2+}$ or $Na^{+}$, since the values reported in the literature for the thicknesses of clay layers saturated with $Ca^{2+}$, $Sr^{2+}$ and $Na^{+}$ for water saturated conditions are very close (14.92, 15.20 and 14.85 Å, respectively; de la Calle and Suquet, 1988). It should be noted that XCa is defined as $XCa = \frac{[Ca]_{sorbed}}{CEC}$ where $[Ca]_{sorbed}$ is the Ca concentration sorbed in the vermiculite in meq/100 $g_{hydrated\ solid}$, as expressed for the CEC (see section 2.1).

In GCMC simulations, the interactions between the different atoms were described using the ClayFF model (Cygan et al., 2004) modified by Ferrage et al. (2011) for the clay layer, and the flexible water SPC model. The Lennard-Jones potentials of the interlayer $Ca^{2+}$ and $Na^{+}$ cations were taken from Cygan et al. (2004), while for $Sr^{2+}$ cations, the potentials used were derived from data in the literature (Aaqvist, 1990), as suggested by Ngouana Wakou (2014). Ewald summation (Heyes, 1994) with 3D periodic boundary conditions was used to reproduce the long-range coulombic potential.

### 2.2.2. Molecular dynamic (MD) simulations

Self-diffusion coefficients of calcium, strontium and sodium were determined by MD simulations, which started from a prior equilibrium configuration obtained by GCMC simulations. Calculations were performed by using the LAMMPS software (Plimpton, 1995). It should be noted that when two types of cations are considered in the interlayer (i.e., $Ca^{2+}$ and $Sr^{2+}$ or $Ca^{2+}$ and $Na^{+}$), the water content used in the structural model has been adjusted using the LAMMPS integrated GCMC algorithm. The microcanonical (NVE, in which N, V and E represent the number of particles, volume and energy, respectively) ensemble was applied for the simulation. A Verlet algorithm (Allen and Tildesley, 1994) was used to obtain the trajectories of the confined cations. The elementary time step employed for the calculations was fixed to 0.5 fs (as in Michot et al., 2012), while the total simulation time of the MD calculations exceeds 2 ns. To stabilize the temperature (T = 298 K) that would otherwise vary over the simulation time, a weakly coupled Berendsen thermostat was used (Berendsen et al., 1954). From the 3D local motions of atoms, the self-diffusion coefficients of the cations (i.e., $D_{self\text{-}interlayer}$) parallel to the clay surface are obtained from the asymptotic slope of the

radial mean squared displacement (see Fig. 1A) defined in the basal plane of the layers according to:

$$D_{self-interlayer} = \frac{1}{4N}\lim_{t\to\infty}\frac{\left(\sum_{i=1}^{N}(x_i(0)-x_i(t))^2+\sum_{i=1}^{N}\left(y_i(0)-y_i(t)\right)^2\right)}{t} \qquad (1)$$

where N is the total number of diffusing cations and *t* is the diffusion time (s). To reduce the statistical noise, calculations were performed by considering four non-overlapping trajectories with a duration of 500 ps extracted from the complete run performed over 2 ns of total simulation time. Finally, self-diffusion coefficients issued from these calculations are dependent only on the environment of the probe in the interlayer space, and are representative of the mobilities of the cations in the interlayer of the bi-hydrated vermiculite, irrespective of the chemical composition of the aqueous reservoir with which vermiculite layers could be in contact.

*2.3 Finite-volume model to simulate the macroscopic exchange rate*

The finite-volume model proposed here to predict the macroscopic dynamics of the cation exchange processes is constrained by the radial self-diffusion coefficients calculated by MD. These coefficients were extracted from the analysis of the ionic trajectories obtained with Eq. (1), and were averaged over the whole atomic structure of the clay/water interface, thus taking into account water and ionic layering (see Fig. 1B) and 3D local mobility of the various atoms. Then, radial-self diffusion coefficients implicitly take into account the limited ionic motions in the direction perpendicular to the clay surface, as reported by Michot et al. (2012). As a consequence, the proposed finite-volume model can simply consider residual 2D macroscopic diffusion of neutral probes freely diffusing on the surface of a structureless

cylindrical section with perfect radial symmetry. In this geometrical configuration, the motion of the probe is described by the one-dimensional radial component of the diffusion equation.

### 2.3.1 Generalities

Radial-cylindrical diffusion with infinite radial symmetry of a probe (i.e., a cation in our case) in a disk can be written as:

$$\frac{\partial C(r,t)}{\partial t} - \frac{1}{r}\frac{\partial}{\partial r}\left(r\,D\frac{\partial C(r,t)}{\partial r}\right) = 0 \qquad (2)$$

where $C(r, t)$ [$ML^{-3}$] is the concentration of the probe at a distance $r$ from the centre of the disk at time $t$ and $D$ [$L^2T^{-1}$] is the diffusion coefficient of the probe in the disk. In this study, $D$ will be taken as the molecular self-diffusion coefficient calculated by MD. From a general standpoint, solving Eq. 2 by relying upon a finite-volume formalism states that for any elementary volume $V$ within the disk, Eq. 2 can be integrated over the volume $V$:

$$\int \frac{\partial C}{\partial t} dV - \int \frac{1}{r}\frac{\partial}{\partial r}\left(rD\frac{\partial C}{\partial r}\right) dV = 0 \qquad (3)$$

where $r^{-1}\,\partial/\partial r(r\,\ldots)$ is the divergent operator in cylindrical coordinates with infinite radial symmetry, and by using the Ostrogradski theorem, Eq. 3 can be rewritten as:

$$\int \frac{\partial C}{\partial t} dV - \int D\frac{\partial C}{\partial r}.n_\Gamma d\Gamma = 0 \qquad (4)$$

where $\Gamma$ is the contour boundary of the volume $V$ and $n_\Gamma$ is the outer normal to the boundary.

Considering the discretisation of the disk with a radial spatial step $\Delta_r$ in concentric cylindrical rings; a ring indexed by $i$ is bound by cylindrical walls located in $(i-1)\Delta_r$ and $i\Delta_r$.

The volume of the ring is $\pi e((i\Delta_r)^2 - ((i-1)\Delta_r)^2)$, where *e* is the thickness of the disk, the diffusing surface-areas of the contours of the ring being $2\pi e i\Delta r$ with a positive outer normal $n_\Gamma$, and $2\pi e(i-1)\Delta r$ with a negative outer normal. By assuming that a uniform mean concentration $C_i$ can be defined over the ring *i*, using a first-order approximation for the spatial derivatives $\partial C/\partial r$, and considering a uniform diffusion coefficient *D* over the disk, Eq. 4 can be discretized as:

$$\frac{C_i^{n+1}-C_i^n}{\Delta t}\pi e\left((i\Delta_r)^2 - \left((i-1)\Delta_r\right)^2\right) - D2\pi e(i\Delta_r)\frac{C_{i+1}^n - C_i^n}{\Delta_r} + D2\pi e(i-1)\Delta_r\frac{C_i^n - C_{i-1}^n}{\Delta_r} = 0 \quad (5)$$

where *n* is the index over the time coordinate discretized at step $\Delta t$. An explicit scheme over time discretizing the spatial derivatives at time $n\Delta t$ is employed. Rearranging Eq. 5 results in:

$$\frac{C_i^{n+1}-C_i^n}{\Delta t}2\Delta_r^2\left(i-\frac{1}{2}\right) = 2Di\left(C_{i+1}^n - C_i^n\right) - 2D(i-1)\left(C_i^n - C_{i-1}^n\right) \quad (6a)$$

i.e.,

$$C_i^{n+1} = C_i^n + \frac{\Delta t\, 2D}{2(\Delta_r)^2\left(i-\frac{1}{2}\right)}\left[i\left(C_{i+1}^n - C_i^n\right) - (i-1)\left(C_i^n - C_{i-1}^n\right)\right] \quad (6b)$$

By denoting $Ne = \frac{D\Delta t}{(\Delta_r)^2}$ (the Von Neumann stability criterion for diffusion; Charney et al., 1950), the concentration of the probe in the *i* concentric ring at time $(n+1)\Delta t$ from those at time *n* is:

$$C_i^{n+1} = \left[\frac{i2Ne}{2i-1}\right]C_{i+1}^n + \left[\frac{(i-1)2Ne}{2i-1}\right]C_{i-1}^n + [1-2Ne]C_i^n \quad (7)$$

It should be noted that to preserve numerical stability, the Von Neumann criterion must be less than 0.5 for the explicit scheme in Eq. 7 to be stable and not subjected to spurious oscillations. It is noteworthy that in Eq. (5) the thickness *e* of the clay particle could be dropped, then rendering the one-dimensional radial diffusion logically independent of the

thickness of the particle. However, in general cases, *e* could be kept in Eq. (5), because one could envision clay particles with non-uniform thickness, or simply boundary conditions at the interface between the particle and the aqueous reservoir that need to be calculated as a ”free” diffusive flux. In that case, the volumes of the clay disk and the reservoir would influence the boundary condition. Finally, note that the preceding reasons also motivate the choice of an explicit numerical solution to simulate the macroscopic diffusion instead of an analytical solution.

### 2.3.2 Input parameters

Since the limited ionic mobility in the direction perpendicular to the clay surface is included in the derivation of the radial self-diffusion coefficient evaluated by MD simulations (see introduction of section 2.3), the macroscopic clay particle is represented in the framework of a finite-volume model by using a simple flat disk with a diameter equal to 5 mm, as used for the experiments. This approximation is justified by results obtained from X-ray diffraction measurements (Walker, 1961; Reed and Scott, 1962 among others) showing that cation exchange reactions occurring in the interlayer of coarse clay particles (i.e. > 10 μm) operate via a radial interlayer diffusion front inside the clay particles. Then, assumption is made that diffusion front moves in the whole particle (i.e., in all layers located in the clay particle) at the same velocity in the radial direction irrespective of the ionic interfacial content. This last approximation is compatible with the results obtained by MD numerical simulations displayed in Fig. 1C exhibiting a limited variation of the radial ionic mobility as a function of the ionic composition of the clay/water interface.

Input parameters of the finite-volume model are as follows: (i) the self-diffusion coefficient, representative of the mobilities of cation inside the particle and generating an interlayer gradient during exchange with the aqueous reservoir, and (ii) the amount of Ca located in the disk and fully exchanged at an infinite time (i.e., amount of initial reactive Ca). Self-diffusion coefficients of interlayer cations were calculated by MD simulations for the structure representative of the clay used experimentally (see section 2.2) and for different $Ca^{2+}/Na^{+}$ and $Ca^{2+}/Sr^{2+}$ interlayer occupancies (i.e., XCa value). Furthermore, amounts of initial reactive Ca were calculated from total amounts of Ca exchanged (i.e., released) at infinite time predicted by means of interlayer selectivity coefficients previously published in Tertre et al. (2013) and Dzene et al. (2016). These total amounts were calculated with the Phreeqc® software (Parkhurst and Appelo, 1999) associated to the thermodynamic database proposed by Johnson et al. (1992) for aqueous species, assuming thermodynamic equilibrium between the solid and aqueous phases with an initial chemical composition representative of the experiments (solid/solution ratio and initial aqueous concentrations for $Na^{+}$, $Ca^{2+}$, $Sr^{2+}$ and $Cl^{-}$ ions). These calculations were performed by considering (i) an interlayer CEC equal to 175 meq/100 $g_{hydrated\text{-}solid}$ as proposed by Dzene et al. (2016) for the same by-hydrated Ca-vermiculite as the one used in this study, and (ii) decimal logarithms of selectivity coefficients (Gaines Thomas convention; Gaines and Thomas, 1953) equal to 0 and 0.1, as proposed by Dzene et al. (2016) and Tertre et al. (2013) describing the exchange in "batch" experiments of $Ca^{2+}$-for-$Sr^{2+}$ and $Ca^{2+}$-for-$Na^{+}$, respectively. As an example, the selectivity coefficient is defined in the case of the $Ca^{2+}$-for-$Na^{+}$ exchange as follow:

$$Kc(Na^{+}/Ca^{2+}) = \frac{E_{Ca2+}[Na^{+}]^{2}_{aq.}\gamma^{2}_{Na+}}{(E_{Na+})^{2}(Ca^{2+})_{aq.}\gamma_{Ca2+}} \quad (8)$$

where $E_{Na+}$ and $E_{Ca2+}$ are the equivalent fractions of $Na^+$ and $Ca^{2+}$ adsorbed in the interlayer, respectively, and, $\gamma_{Na+}$ and $\gamma_{Ca2+}$ are the activity coefficients for $Na^+$ and $Ca^{2+}$ aqueous species calculated by using the Davies approximation (Davies, 1962). Brackets indicate the concentrations of the species in solution at equilibrium (mol/$kg_{water}$).

Table 1 reports on the % of Ca (normalised to the sample CEC) released in solution and calculated at infinite time (i.e., thermodynamic equilibrium) for the different studied systems. Using CEC sample and solid/solution ratio, these values are then converted into the total amounts of Ca released in solution at infinite time and are assumed to be equal to the total amounts of reactive Ca initially located in the disk (see values in Table 1). For each system, this amount is then distributed between *i* concentric rings according to the spatial discretisation chosen for the disk ($i.e.,\Delta_r$; see section 2.3.1). Preliminary results reported in Supporting Material 1 (S.M.1; available online) showed that the simulated data were no longer dependent on the number of the concentric rings when this number was above 8 (see Fig. S.M.1). These data were obtained by considering an interlayer diffusion coefficient equal to $5.0x10^{-12}$ $m^2 \cdot s^{-1}$ (corresponding to the self-diffusion coefficient calculated by MD for $Ca^{2+}$ when XCa = 1 for $Sr^{2+}$for-$Ca^{2+}$ exchange; see section 3.1) and a % of Ca (normalised to sample CEC) released in solution at infinite time equal to 100%. According to these results, all subsequent calculations were performed by considering a spatial discretisation using 8 rings, corresponding to take a radial step of 0.3125 mm ($\Delta_r$), with the whole reproducing the actual radius (i.e., 2.5 mm) of the particle used in the experiments. It should be noted that the initial amount of Ca present in each concentric ring was set up to keep a uniform concentration over the entire disk irrespective of the volume (surface in 2-D) of each ring. Then, using this method, the amount of initial Ca present in each ring varies in order to respect the variation of the surface between the different rings. Furthermore, it should be

noted that considering an initial amount of Ca in the disk different from that calculated by assuming a full exchange at infinite time in some cases (see Table 1) can be viewed as an effect of a limitation existing at the clay/water interface due to too low of amounts of $Na^+$ or $Sr^{2+}$ cations in the aqueous reservoir to exchange all $Ca^{2+}$ cations at infinite time. Finally, whatever the diffusion time investigated and experiment simulated, the outer boundary condition of the disk (i.e., amount of Ca considered at the external part of the larger concentric ring) was set to zero, a value simulating an infinite dilution of the Ca released by the disk into a large aqueous reservoir.

## 3. Results and Discussion

### *3.1 Simulation of molecular self-diffusion coefficients*

Irrespective of the $Ca^{2+}/Sr^{2+}$ and $Ca^{2+}/Na^+$ interlayer occupancies (i.e., XCa; see section 2.2.1) used to perform the GCMC simulations, two types of populations for the three types of cations investigated (i.e., $Ca^{2+}$, $Sr^{2+}$ and $Na^+$) can be observed. Indeed, one cationic population is located in the middle plane of the interlayer (z-position close to 0 Å), while another one prevails close to the clay surface (at approximately 2 Å from the interlayer middle plane). This behaviour, in agreement with previous results (Tertre et al., 2015), is illustrated in Fig. 1B for the organization of $Ca^{2+}$ and $Sr^{2+}$ for XCa = 0.5 and for $Ca^{2+}$ and $Na^+$ for XCa = 0.5, respectively. For each value of XCa tested, the self-diffusion coefficient of each cation was obtained from the averaged mean-squared displacements obtained over the different populations (see Fig. 1A). These values are reported as a function of XCa in Fig. 1C for $Sr^{2+}/Ca^{2+}$ and $Na^+/Ca^{2+}$. Self-diffusion coefficients of both $Ca^{2+}$ and $Sr^{2+}$ cations can be considered as being independent of XCa during $Sr^{2+}$-for-$Ca^{2+}$ exchange (see Fig. 1C) with

average values (within one standard deviation) equal to $4.0\pm0.6\times10^{-12}$ and $5.0\pm0.6\times10^{-12}$ $m^2 \cdot s^{-1}$ for $Sr^{2+}$ and $Ca^{2+}$, respectively. On the other hand, during $Na^+$-for-$Ca^{2+}$ exchange, the self-diffusion coefficient of $Na^+$ is divided by approximately a factor 2 when XCa increases from 0 to 1, with the self-diffusion coefficient of $Ca^{2+}$ being for its part rather constant at $5.5\pm1.9\times10^{-12}$ $m^2 \cdot s^{-1}$ (see Fig. 1C). The latter value, up to the addition of its standard deviation, is in good agreement with the $8\pm1.2\times10^{-12}$ $m^2 \cdot s^{-1}$ average value proposed by Tertre et al. (2015) for $Ca^{2+}$ in the interlayer of a similar bi-hydrated structure.

*3.2 Comparison between experimental data and prediction of the finite-volume model*

The finite-volume model proposed in this study is based only on a single diffusion coefficient (see Eq. 2 and definition of the Von Neumann stability criterion in section 2.3.1). Firstly, assumption is made that, irrespective of the pair of cations studied, exchange can be depicted by using a self-diffusion coefficient corresponding to the average value of the slowest cation present in the system (i.e., within the range of XCa investigated, $Sr^{2+}$ in the $Sr^{2+}$-for-$Ca^{2+}$ exchange and $Ca^{2+}$ in the $Na^+$-for-$Ca^{2+}$ exchange, see section 3.1). These assumptions suggest that the slowest interlayer cation controls the dynamics of ion-exchange between the interlayer of the swelling clay mineral and the aqueous reservoir. With this assumption, the interlayer diffusion coefficients *D* used in Eq. 2 are set to $4.0\pm0.6\times10^{-12}$ and $5.5\pm1.9\times10^{-12}$ $m^2 \cdot s^{-1}$ (see Fig. 1C) to describe $Sr^{2+}$-for-$Ca^{2+}$ and $Na^+$-for-$Ca^{2+}$ exchanges, respectively. Calculations of radial diffusion by the finite-volume model accounting for both of the above diffusion coefficients and a uniform initial concentration of Ca in the disk (see Table 1) are compared to experimental data in Fig. 2A and 2B for the cases of $Sr^{2+}$-for-$Ca^{2+}$ and $Na^+$-for-$Ca^{2+}$ exchanges and for different salinities of the aqueous reservoir. It should be noted that logarithm representations are used in Fig. 2 to better

analyse the entire time-range investigated. As expected, the % Ca released in solution increases with both the salinity of the aqueous reservoir and diffusion time. It should be noted that for the $Sr^{2+}$-for-$Ca^{2+}$ experiment, a salinity reservoir equal to $10^{-2}$ mol/$kg_{water}$ in $SrCl_2$ allows to reach a complete release in the aqueous solution of the confined calcium at infinite time, while for $Na^{+}$-for-$Ca^{2+}$, the complete release is obtained for a salinity of the aqueous reservoir dramatically higher at 1 mol/$kg_{water}$ NaCl. This behaviour is in agreement with selectivity coefficients previously published and describing the adsorption of these cations in swelling clay minerals (Wild and Keay, 1964).

As far as the $Sr^{2+}$-for-$Ca^{2+}$ exchange is concerned, a good agreement is obtained between experimental and predicted data irrespective of the salinity of the aqueous reservoir tested. Regarding the $Na^{+}$-for-$Ca^{2+}$ exchange, a good agreement is also obtained for the lowest salinity condition (i.e., $3x10^{-3}$ mol/$kg_{water}$), whereas the model overestimates by approximately 20% and underestimates by approximately 15% the data measured for the intermediate (i.e., $5x10^{-2}$ mol/$kg_{water}$) and highest (i.e., 1 mol/$kg_{water}$) salinity conditions, respectively. Then, based on self-diffusion coefficients obtained by MD and selectivity coefficients classically obtained from “batch” data at equilibrium, the maximum difference between the experimental and simulated data is only 20%, which is very satisfying because the diffusion model makes the link between the molecular and millimetre-scale processes. This upscaling approach based on continuous equations and consisting of predicting the dynamics of the cation-exchange reaction at the macroscopic scale seems to be rather robust. In the following, the results from tests of sensitivity are presented to collect more insights into the parameters (i.e., self-diffusion coefficient and selectivity coefficient) controlling the dynamics of the macroscopic ion-exchange rates.

*3.3 Sensitivity of the finite-volume model to the self-diffusion coefficients and selectivity coefficients applied for $Na^+$-for-$Ca^{2+}$ exchange*

Simulated data are dependent on the averaged values chosen for both self-diffusion and cation-exchange selectivity coefficients used as input parameters in the finite-volume model. In this section, the sensitivity of the simulated data to these two non-coupled coefficients is then discussed, especially by fixing one of the coefficients and by varying the other one. For self-diffusion, the calculations were performed for the $Na^+$-for-$Ca^{2+}$ exchange because the self-diffusion coefficients of both $Ca^{2+}$ and $Sr^{2+}$ are almost the same considering the standard deviations associated with their mean values (i.e., $Ca^{2+}$ with $5.0\pm0.6\text{x}10^{-12}$ and $Sr^{2+}$ with $4.0\pm0.6\text{x}10^{-12}$ $m^2 \cdot s^{-1}$). In turn, this characteristic prohibits the detection of significant differences between data simulated by considering the average values of both cations or of the smallest ones (comparison not shown). Regarding selectivity coefficients, sensitivity calculations are also performed for the $Na^+$-for-$Ca^{2+}$ exchange because the average value over the XCa range of the $\log K_c(Ca^{2+}/Sr^{2+})$ allows for interpreting the dynamics of the $Sr^{2+}$-for-$Ca^{2+}$ exchange in millimetre disks for all salinity conditions investigated. It is however reminded that the average value of the $\log K_c(Na^+/Ca^{2+})$ overestimates by approximately 20% the experimental data obtained for intermediate salinity conditions (i.e., $5\text{x}10^{-2}$ $mol/kg_{water}$) (see discussion in section 3.2).

3.3.1 Sensitivity to self-diffusion coefficients

For the 1 $mol/kg_{water}$ NaCl condition, a maximum deviation between experimental and simulated data of 15% (see Fig. 2B) can be observed, especially for short diffusion times

(i.e., <2 days). This part of the simulated curve is highly sensitive to the self-diffusion coefficient used in the calculation. This value was previously assumed to be equal to the average value of the self-diffusion coefficient of the slowest cation (i.e., $Ca^{2+}$) involved in the studied system over the entire XCa range investigated (i.e., $5.5\pm1.9\times10^{-12}$ $m^2 \cdot s^{-1}$). To test the sensitivity of the simulated data to this parameter, two additional calculations were performed for the 1 $mol/kg_{water}$ and $3\times10^{-3}$ $mol/kg_{water}$ salinity conditions by using self-diffusion coefficients equal to $1.3\times10^{-11}$ and $2.1\times10^{-11}$ $m^2 \cdot s^{-1}$. The value of $1.3\times10^{-11}$ corresponds to averaging between the diffusion coefficients of both $Ca^{2+}$ and $Na^{+}$ over the XCa range, while the value $2.1\times10^{-11}$ corresponds to averaging the diffusion of the most mobile cation (i.e., $Na^{+}$ in this case) over the XCa range (see Fig. 1C). The comparison between the simulated curves and experimental data is presented in Fig. 3. On the one hand, the self-diffusion coefficient equal to $1.3\times10^{-11}$ $m^2 \cdot s^{-1}$ is able to interpret experimental data obtained with 1 $mol/kg_{water}$ and $3\times10^{-3}$ $mol/kg_{water}$ salinity conditions (by accounting for uncertainties in the experimental data) for all diffusion times investigated. On the other hand, the value of $2.1\times10^{-11}$ $m^2 \cdot s^{-1}$ interprets experimental data obtained for the 1 $mol/kg_{water}$ salinity condition at short times but not at intermediate times (i.e., a few days), and it systematically overestimates the data measured for the $3\times10^{-3}$ $mol/kg_{water}$ salinity condition at diffusion times smaller than a few days (see Fig. 3). Therefore, choosing the $1.3\times10^{-11}$ $m^2 \cdot s^{-1}$ value, corresponding to the average value of the self-diffusion coefficients of both cations, appears to be the best option to interpret the entire set of experimental data for all of the salinities experienced in the aqueous reservoir.

These results highlight that for an exchange involving two cations with significantly different molecular mobilities, the average value of both interlayer diffusion coefficients, irrespective of the XCa value, is certainly the best compromise. However, it worth noting

that interlayer diffusion coefficients of both $Ca^{2+}$ and $Na^{+}$ only differ by a factor of 2.3. In the case of competitions between other types of cations such as $Cs^{+}$ and $Na^{+}$ for which mobility contrast is enhanced due to significant variation in the interlayer structures of the two-end members (Bourg and Sposito, 2010; Porion et al., 2015 among others), the average value could eventually render flawed results.

3.3.2 Sensitivity to the selectivity coefficient

In section 3.2, calculations were performed by considering that the selectivity coefficient describing ion-exchange in the interlayer of vermiculite was independent of both the particle size and the physico-chemical parameters (e.g., compositions of both the clay interlayer and aqueous composition at equilibrium). It should be noted however, that even though this parameter was found to be independent of the size fraction in the case of the $Sr^{2+}$-for-$Ca^{2+}$ for three size fractions (i.e., 0.1-0.2, 1-2 and 10-20 µm; Dzene et al., 2016), the question of variability with the particle size remains in the case of the $Na^{+}$-for-$Ca^{2+}$ exchange since the authors (Tertre et al., 2013) worked only on a <150 µm size fraction. To assess the validity of such an assumption, additional data were obtained in this present study in batch experiments with a coarser size fraction of vermiculite (i.e., 50-150 µm). These data were obtained by following a methodology detailed in Tertre et al. (2011) and are reported in S.M.2 with the associated interpretation. These data allow for confirming the independence of the interlayer selectivity coefficient in the case of the $Na^{+}$-for-$Ca^{2+}$ exchange with the particle size (i.e., $\log K_c(Na^{+}/Ca^{2+})$ = 0.1 using the Gaines Thomas convention). In addition, these data also show that a high uncertainty exists in the $\log K_c(Na^{+}/Ca^{2+})$ value for physicochemical conditions close to homoionic solution (i.e., for $\{Na^{+}\}_{aq.}>0.999$ with $\{Na^{+}\}_{aq.}$ the equivalent fraction of $Na^{+}$ in solution at equilibrium) since a range of $\log K_c(Na^{+}/Ca^{2+})$

values from 0.1 to 1.3 is able to interpret experimental data for such conditions (see details in S.M.2). This behaviour differs from that considering a unique selectivity coefficient value to predict $Ca^{2+}$-for-$Na^{+}$ interlayer exchange, irrespective of the physicochemical conditions used (e.g., for $0<\{Na^{+}\}_{aq.}<1$).

In Fig. 4, the prediction of the finite-volume model parameterized with the highest possible interlayer selectivity coefficient (i.e., $\log K_c(Na^{+}/Ca^{2+}) = 1.3$) describing $Ca^{2+}$-for-$Na^{+}$ exchange in "batch conditions" when $\{Na\}_{aq.} >0.999$ (corresponding to the $5x10^{-2}$ $mol/kg_{water}$ NaCl condition in this study) is compared to the experimental data. Calculations were performed by considering the average self-diffusion coefficient of the slowest cation in the whole XCa range (i.e., $Ca^{2+}$ with $D_{self\text{-}interlayer} = 5.5x10^{-12}$ $m^2 \cdot s^{-1}$), as for the data reported in Fig. 2. In Fig. 4, a good agreement can be observed between experimental and simulated data for this $\{Na\}_{aq.} >0.999$ condition. This behaviour confirms the observation previously discussed regarding the limitation associated with the use of the same selectivity coefficient to describe the ion-exchange reaction irrespective of the physico-chemical conditions. This limitation is emphasized, especially when the system is close to that of homoionic solid and aqueous phases and even for a pair of cations allowed to maintain the same interlayer hydration during ion-exchange reactions (i.e., by-hydrated structure in our case). Furthermore, for the 1 M NaCl condition, simulated data using a $\log K_c(Na^{+}/Ca^{2+})$ value equal to 1.3 are perfectly superimposed to those simulated with the average selectivity coefficient previously tested (i.e., $\log K_c(Na^{+}/Ca^{2+}) = 0$) (see Fig. 4). For their part, experimental data obtained at the lowest salinity (i.e., $3x10^{-3}$ $mol/kg_{water}$) can be interpreted only by relying upon an average selectivity coefficient value of $\log K_c(Na^{+}/Ca^{2+}) = 0.1$. This observation is in agreement with the usual methodology reputed to lower uncertainties (Tournassat et al.,

2007; Tertre et al., 2011) and consistent to obtain selectivity coefficients for systems far removed from homoionic conditions (in both solid and aqueous phases).

These sensitivity calculations confirm the robustness of the approach proposed in this work, employing an average selectivity coefficient between the two cations over the XCa range investigated under the acceptation that a maximum deviation of 20% between experimental and simulated data is tolerable. It is worth noting that these sensitivity calculations, based on the consideration of a unique selectivity coefficient, fully ignore potential effects related to the release of $Ca^{2+}$ cations in the aqueous reservoir due to the ongoing ion-exchange process. This is an implicit property of the simple model used here, in contrast to existing more sophisticated coupled models, which would likely lead to an overestimation of the calculated ion-exchange rate compared to experimental data. As seen from the good agreement between the experiments and simulations, this effect is likely to be considered as marginal for the experimental conditions used here.

## 4. Concluding remarks and perspectives

The results obtained in this study showed that self-diffusion coefficients obtained by molecular dynamic simulations can successfully be used to interpret cation-exchange laboratory experiments despite the large gap, in terms of timescale, between the two methods. Moreover, this study allowed to assess with a finite-volume model based on a continuous diffusion equation and a single diffusion coefficient the role played by both self-diffusion coefficients and selectivity coefficients in the dynamics of the ion-exchange reaction between the interlayer of individual swelling clay mineral particles and aqueous reservoirs characterised by contrasted chemical compositions. The results showed that the dynamics of a macroscopic exchange was mainly ruled by the interlayer mobility of the

slowest cation in the ion-exchange investigated. Cation-exchange selectivity coefficient appeared to be independent of the particle size when the hydration state of the clay particle interlayer is kept constant during the exchange reaction. This behaviour was previously reported in the case of $Sr^{2+}$-for-$Ca^{2+}$ exchange in batches for three vermiculite size fractions (0.1-0.2, 1-2 and 10-20 µm; Dzene et al., 2016)). It was extended here to the $Ca^{2+}$-for-$Na^{+}$ exchange, with data obtained using a <150 µm size fraction able to interpret data obtained with millimetre particles. This notwithstanding, sensitivity calculations showed a noticeable uncertainty in the selectivity coefficient for conditions close to a homoionic system (in both solid and aqueous phases). Consequently, even for two cations preserving the structure of the interlayer space during their exchange in water saturated conditions, using a unique selectivity coefficient to describe the ion-exchange reaction irrespective of the chemical composition of the system remains questionable. Finally, MD simulations showed that the self-diffusion coefficient of an interlayer cation could vary as a function of its occupancy in the interlayer (i.e., the case of $Na^{+}$ in the present study). These data can be, at least qualitatively, interesting for reactive transport models coupling chemistry to transport in order to assess the role played by the different parameters in the global diffusion process investigated.

The interpretation raised from this study were based using a large range of salinities for the aqueous reservoir (from approximately a few $10^{-5}$ to 1 mol/$kg_{water}$) and for two pairs of cations differing by their charge (i.e., divalent/divalent cations and monovalent/divalent cations) allowing to keep the interlayer structure unchanged during exchange (i.e., by-hydrated structure in water saturated conditions). Then, possible perspective of this work could be related to the study of the exchange for a cationic duo inducing a change in the structure (e.g, hydration state) of the interlayers of vermiculite during ion-exchange

reactions (e.g., $Cs^+$-for-$Na^+$; Dzene et al., 2015 and 2017), thus impacting then self-diffusion and selectivity coefficients. Furthermore, extension of the proposed model to other types of swelling clay minerals, as smectites, would likely imply to change the input parameters, such as self-diffusion coefficients and selectivity coefficients, due to the different layer charges of these minerals. This modelling approach could thus help in assessing the role played by layer charge on the kinetics of cation-exchange process, especially for smectites for which the experiments as those proposed in this study are impossible due to their small particle sizes. Finally, the results obtained in this present study here, for diluted systems (i.e., low solid/solution ratio), could be taken into account in reactive transport models devoted to simulating ion-exchange reactions during the diffusion of cations in porous clay media (i.e., high solid/solution ratio), for which the proportion of interlayer porosity can be known.

**Acknowledgements**

Hugo Petit (IC2MP/HydrASA, Poitiers, France) is thanked for his experimental contribution to the $Ca^{2+}$-for-$Na^+$ isotherm measurement performed with the 50-150 µm size fraction. The authors are grateful to the EC2CO CNRS/INSU BIOHEFECT project (Project DIFFMATARG) and the European Union (ERDF) and "Région Nouvelle Aquitaine" for providing the financial support for this study.

**Figure captions**

Figure 1: Results from GCMC and MD simulations. (A) Asymptotic slope of the radial mean squared displacement obtained for the cations with XCa = 0.5. (B) Interlayer atomic density profiles (in atoms/Å$^3$) of cations for XCa = 0.5. (C) Variation of the self-diffusion coefficients of cations as a function of XCa. XCa is the equivalent fraction of $Ca^{2+}$ in the interlayer. In Fig. 1C, dashed lines represent the average self-diffusion coefficients of $Ca^{2+}$ and $Sr^{2+}$ over a XCa range from 0 to 1. Left and right columns report on the data for $Sr^{2+}$-for-$Ca^{2+}$and $Na^{+}$-for-$Ca^{2+}$ exchanges, respectively.

Figure 2: Evolution over the diffusion time of the experimental % of Ca released in the solution normalised to the sample CEC (symbols) and compared with the simulations by the finite-volume model (solid and dashed lines). The average value over the XCa range of the self-diffusion coefficient of the slowest cation was used for the simulations. Solid lines report on calculations with this mean value, while dashed lines draw the envelope associated with coefficients defined up to their standard deviation. (A) $Sr^{2+}$-for-$Ca^{2+}$; (B) $Na^{+}$-for-$Ca^{2+}$.

Figure 3: Effect of the self-diffusion coefficient value used in the finite-volume model to predict $Na^{+}$-for-$Ca^{2+}$ dynamic exchange with millimetre disks. Simulated data (lines) are performed for the 1 mol/kg$_{water}$ and 3x10$^{-3}$ mol/kg$_{water}$ NaCl conditions and are compared to the experimental data (symbols).

Figure 4: Effects of a log$K_c$($Na^{+}$/$Ca^{2+}$) equal to 1.3 (i.e., the highest possible selectivity coefficient interpreting batch data for {Na}$_{aq.}$ >0.999; see Fig. S.M.2B and details in S.M.2) on simulations of exchange rates versus the diffusion time via the finite-volume model for disks immersed in 5x10$^{-2}$ mol/kg$_{water}$ NaCl solution.

Dots correspond to experimental data (Fig. 2). All dashed lines represent simulated data using the average self-diffusion coefficient of the slowest cation in the entire XCa range (i.e., $Ca^{2+}$ with $D_{self\text{-}interlayer}$ = $5.5x10^{-12}$ $m^2.s^{-1}$). The solid line reports simulated data for the 1 $mol/kg_{water}$ salinity condition using a self-diffusion coefficient as the mean between mean coefficients of both $Na^+$ and $Ca^{2+}$ (i.e., $1.3x10^{-11}$ $m^2{\cdot}s^{-1}$; see text for details).

**Table caption:**

Table 1: Chemical compositions of the initial solutions used in the experiments and those predicted at infinite time with Phreeqc® software (Parkhurst and Appelo, 1999) assuming a thermodynamic equilibrium after ion-exchange reactions. These simulated data are converted in % of Ca (normalised to the sample CEC) released in solution at infinite time, and in amounts of initial reactive Ca in the vermiculite used as input parameters in the finite-volume model proposed.

**References**

Aaqvist, J., 1990. Ion-water interaction potentials derived from free energy perturbation simulations. J. Phys. Chem. 94, 8021–8024. http://dx.doi.org/10.1021/j100384a009.

Allen, M.P., Tildesley, D.J., 1994. Computer Simulation of Liquids. Clarendon Press, Oxford.

Appelo, C. A. J., Wersin, P., 2007. Multicomponent diffusion modeling in clay systems with application to the diffusion of tritium, iodide, and sodium in Opalinus clay. Environ. Sci. Technol. 41, 5002–5007. https://doi.org/10.1021/es0629256

Appelo, C.A.J., Van Loon, L.R., Wersin, P., 2010. Multicomponent diffusion of a suite of tracers (HTO, Cl, Br, I, Na, Sr, Cs) in a single sample of Opalinus clay. Geochim. Cosmochim. Acta 74, 1201-1219. https://doi.org/10.1016/j.gca.2009.11.013

Argüelles, A., Leoni, M., Blanco, J. A., Marcos, C., 2010. Semi-ordered crystalline structure of the Santa Olalla vermiculite inferred from X-ray powder diffraction. Am. Mineral. 95, 126–134. https://doi.org/10.2138/am.2010.3249

Berendsen, H.J.C., Postma, J.P.M., Van Gunsteren, W.F., DiNola, A., Haak, J.R.J., 1984. Molecular dynamics with coupling to an external bath J. Chem. Phys. 81, 3684-3690. https://doi.org/10.1063/1.448118

Birgersson, M., Karnland, O., 2009. Ion equilibrium between montmorillonite interlayer space and an external solution – Consequences for diffusional transport. Geochim. Cosmochim. Acta 73, 1908-1923. https://doi.org/10.1016/j.gca.2008.11.027

Bourg, I.C., Bourg, A.C.M., Sposito, G., 2003. Modeling diffusion and adsorption in compacted bentonite: a critical review. J. Contam. Hydrol. 61, 293-302. https://doi.org/10.1016/S0169-7722(02)00128-6

Bourg, I.C., Sposito, G., 2010. Connecting the molecular scale to the continuum scale for diffusion processes in smectite-rich poroux media. Environ. Sci. Techn. 44, 2085-2091. https://doi.org/10.1021/es903645a

Charlet, L., Alt-Epping, P., Wersin, P., Gilbert., B., 2017. Diffusion transport and reaction in clay rocks: a storage (nuclear waste, $CO_2$, $H_2$), energy (shale gas) and water quality issue. Advances Water Research 106, 39-59. https://doi.org/10.1016/j.advwatres.2017.03.019

Charney, J.G., Fjortoft, R., Von Neumann, J., 1950. Numerical integration of the barometric vorticity equation. Tellus 2, 237-254. https://doi.org/10.1111/j.2153-3490.1950.tb00336.x

Cygan, R. T., Liang, J. J., Kalinichev, A. G., 2004. Molecular models of hydroxide, oxyhydroxide and clay phases and the development of a general force field. J. Phys. Chem. B 108, 1255–1266. https://doi.org/10.1021/jp0363287

Dabat, T., Porion, P., Hubert, F., Paineau, E., Dazas, B., Grégoire, B., Tertre, E., Delville, A., Ferrage, E., 2020. Influence of preferred orientation of clay particles on the diffusion of water in kaolinite porous media at constant porosity. In press, Applied Clay Science. https://doi.org/10.1016/j.clay.2019.105354

Davies, C.W., 1962. Ion Association. Butterworth, London.

de la Calle, C., Suquet, H., 1988. Vermiculite, in: Bailey, S.W. (Ed.), Hydrous Phyllosilicates (exclusive of micas). Reviews in Mineralogy Volume 19. Mineralogical Society of America, Chantilly, VA, pp. 455–496.

Delville, A., 1991. Modeling the clay-water interface. Langmuir 7, 547-555. https://doi.org/10.1021/la00051a022

Dzene, L., Tertre, E., Hubert, F., Ferrage, E., 2015. Nature of the sites involved in the process of cesium desorption from vermiculite. J. Colloid Interface Sci. 455, 254–260. https://doi.org/10.1016/j.jcis.2015.05.053

Dzene, L., Ferrage, E., Hubert, F., Delville, A., Tertre, E., 2016. Experimental evidence of the contrasting reactivity of external vs. interlayer adsorption sites on swelling clay minerals: the Case of $Sr^{2+}$-for-$Ca^{2+}$ exchange in vermiculite. Appl. Clay Sci. 132-133, 205-215. https://doi.org/10.1016/j.clay.2016.06.007

Dzene, L., Verron, H., Delville, A., Michot, L.J., Robert, J.L., Tertre, E., Hubert, F., Ferrage, E., 2017. Influence of tetrahedral layer charge on the fixation of cesium in synthetic smectite. J. Phys. Chem. C 121, 23422–23435. https://doi.org/10.1021/acs.jpcc.7b06308

Ferrage, E., Sakharov, B.A., Michot, L.J., Delville, A., Bauer, A., Lanson, B., Grangeon, S., Frapper, G., Jiménez-Ruiz, M., Cuello, G.J., 2011. Hydration properties and interlayer organization of water and ions in synthetic Na-smectite with tetrahedral layer charge. Part 2.

Toward a precise coupling between molecular simulations and diffraction data. J. Phys. Chem. C 115, 1867–1881. https://doi.org/10.1021/jp105128r

Gaines, G.L., Thomas, H.C., 1953. Adsorption studies on clay minerals. II. A formulation of the thermodynamics of exchange adsorption. J. Chem. Phys. 21, 714. https://doi.org/10.1063/1.1698996

Glaus, M. A., Baeyens, B., Bradbury, B., Jakob, A., Van Loon, L.R., Yaroshchuk, A., 2007. Diffusion of $^{22}$Na and $^{85}$Sr in montmorillonite: Evidence of interlayer diffusion being the dominant pathway at high compaction. Environ. Sci. Technol. 41, 478–485. https://doi.org/10.1021/es061908d

Heyes, D.M., 1994. Pressure tensor of partial-charge and point-dipole lattices with bulk and surface geometries. Phys. Rev. B Cond. Matt. 49, 755-764. https://doi.org/10.1103/PhysRevB.49.755

Johnson, J.W., Oelkers, E.H., Helgeson, H.C., 1992. SUPCRT92: a software package for calculating the standard molars thermodynamic properties of minerals, gases, aqueous species and reactions from 1 to 5000 bars and 0 to 1000°C. Comput. Geosci. 18, 899-947. https://doi.org/10.1016/0098-3004(92)90029-Q

Jougnot, D., Revil, A., Leroy, P., 2009. Diffusion of ionic tracers in the Callovo-Oxfordian clay–rock using the Donnan equilibrium model and the formation factor. Geochim. Cosmochim. Acta 73, 2712–2726. https://doi.org/10.1016/j.gca.2009.01.035

Lajunen L.H.J., Peramaki P., 2004. Spectrochemical Analysis by Atomic Absorption and Emission. Cambridge Royal Society of Chemistry.

Marry, V., Turcq, P., 2003. Microscopic simulations of interlayer structure and dynamics in bihydrated heteroionic montmorillonites. J. Phys. Chem. B. 107, 1832-1839. https://doi.org/10.1021/jp022084z

Michot, L.J., Ferrage, E., Jimenez-Ruiz, M., Boehm, M., Delville, A., 2012. Anisotropic features of water and ion dynamics in synthetic Na- and Ca-smectites with tetrahedral layer charge. A combined quasi-elastic neutron-scattering and molecular dynamics simulations study. J. Phys. Chem. C 116, 16619-16633. https://doi.org/10.1021/jp304715m

Ngouana Wakou, B.F., 2014. Modélisation moléculaire de l'hydratation, de la Structure, et de la mobilité des Ions et de l'eau dans l'espace Interfoliaire et à la Surface d'une argile smectitique (Ph.D. Thesis from Ecole des Mines de Nantes (in French)).

Parkhurst, D.L., Appelo, C.A.J., 1999. Phreeqc2 user's manual and program, US Geological Survey. Available at: https://www.usgs.gov/software/phreeqc-version-3

Parkhurst, D.L., Appelo, C.A.J., 2013. Description of input and examples for PHREEQC Version 3 - a computer program for speciation, batch-reaction, one-dimensional transport, and inverse geochemical calculations. U.S. Geological Survey Techniques and Methods, book 6, chap. A43, 497 p., available at http://pubs.usgs./gov/tm/06/a43/

Plimpton, S., 1995. Fast parallel algorithms for short-range molecular dynamics. J. Comp. Phys. 117, 1-19. https://lammps.sandia.gov

Porion, P., Warmont, F., Faugère, A.M., Rollet, A.L., Dubois, E., Marry, V., Michot, L.J., Delville, A., 2015. 133Cs nuclear magnetic resonance relaxometry as a probe of the mobility of cesium cations confined within dense clay sediments. Journal of Physical Chemistry C 119, 15360-15372. https://doi.org/10.1021/acs.jpcc.5b03880

Reed, M.G., Scott, A.D., 1962. Kinetics of potassium release from biotite and muscovite in sodium tetraphenylboron solutions. Soil Science Society Proceeding 26, 437-440.

Steefel, C.I., Appelo, C.A.J., Arora, B., Jacques, D., Kalbacher, T., Kolditz , O., Lagneau, V., Lichtner, P.C., Mayer, K.U., Meeussen, J.C.L., Molins, S., Moulton, D., Shao, H., Simunek, J., Spycher, N., Yabusaki, S.B., Yeh, G.T., 2015. Reactive transport codes for subsurface environmental simulation. Comput. Geosci. 19, 445-478. https://doi.org/10.1007/s10596-014-9443-x

Tachi, Y., Yotsuji, K., 2014. Diffusion and sorption of Cs+, Na+, I- and HTO in compacted sodium montmorillonite as a function of porewater salinity: integrated sorption and diffusion model. Geochim. Cosmochim. Acta 132, 75–93. https://doi.org/10.1016/j.gca.2014.02.004

Tachi, Y., Yotsuji, K., Suyama, T., Ochs, M., 2014. Integrated sorption and diffusion model for bentonite. Part 2. Porewater chemistry, sorption and diffusion modeling in compacted systems. J. Nucl. Sci. Technol. 51, 1–14. https://doi.org/10.1080/00223131.2014.914453

Tertre, E., Prêt, D., Ferrage, E., 2011. Influence of the ionic strength and solid/solution ratio on Ca(II)-for-$Na^{+}$ exchange in montmorillonite. Part 1 : Chemical measurements, thermodynamic modeling and implications for trace elements geochemistry. J. Colloid Interface Sci. 353, 248-256. https://doi.org/10.1016/j.jcis.2010.09.039

Tertre, E., Hubert, F., Bruzac, S., Pacreau, M., Ferrage, E., Prêt, D., 2013. Ion-exchange reactions on clay minerals coupled with advection/dispersion processes. Application to $Na^{+}/Ca^{2+}$ exchange on vermiculite: Reactive-transport modeling, batch and stirred flow-through reactor experiments. Geochim. Cosmochim. Acta 112, 1-19. http://dx.doi.org/10.1016/j.gca.2013.02.028

Tertre, E., Delville, A., Prêt, D., Hubert, F., Ferrage, E., 2015. Cation diffusion in the interlayer space of swelling clay minerals - a combined macroscopic and microscopic study. Geochim. Cosmochim. Acta 149, 251–267. http://dx.doi.org/10.1016/j.gca.2014.10.011.

Tinnacher, R.M., Holmboe, M., Tournassat, C., Bourg, I.A., Davis, J.A., 2016. Ion adsorption and diffusion in smectite: molecular, pore and continuum scale views. Geochim. Cosmochim. Acta 177, 130-149. https://doi.org/10.1016/j.gca.2015.12.010

Tournassat, C., Gailhanou, H., Crouzet, C., Braibant, G., Gautier, A., Lassin, A., Blanc, P., Gaucher, E.C., 2007. Two cation exchange models for direct and inverse modelling of solution major cation composition in equilibrium with illite surfaces, Geochim. Cosmochim. Acta 71, 1098-1114. https://doi.org/10.1016/j.gca.2006.11.018

Tournassat, C., Chapron, Y., Leroy, P., Boulahya, F., 2009. Comparison of molecular dynamics simulations with triple layer and modified Gouy-Chapman models in a 0.1 M NaCl – montmorillonite system. J. Colloid Interface Sci. 339, 533–541. https://doi.org/10.1016/j.jcis.2009.06.051

Tournassat, C., Steefel, C. I., 2015. Ionic transport in nanoporous clays with consideration of electrostatic effects. Rev. Mineral. Geochem. 80, 287–330. https://doi.org/10.2138/rmg.2015.80.09

Tournassat, C., Steefel, C.I., 2019. Modeling diffusion processes in the presence of a diffuse layer at charged mineral surfaces: a benchmark exercise. Comput. Geosci. https://doi.org/10.1007/s10596-019-09845-4

Walker, G.G., 1961. Vermiculite minerals. Ch. 7 in the X-ray identification and crystals structures of clay minerals (G. Brown, ed.). Mineralogical Society, London.

Wild, A., Keay, J., 1964. Cation exchange equilibria with vermiculite. J. Soil Sci. 15, 135–144. http://dx.doi.org/10.1111/j.1365-2389.1964.tb02214.x.

Fig. 1

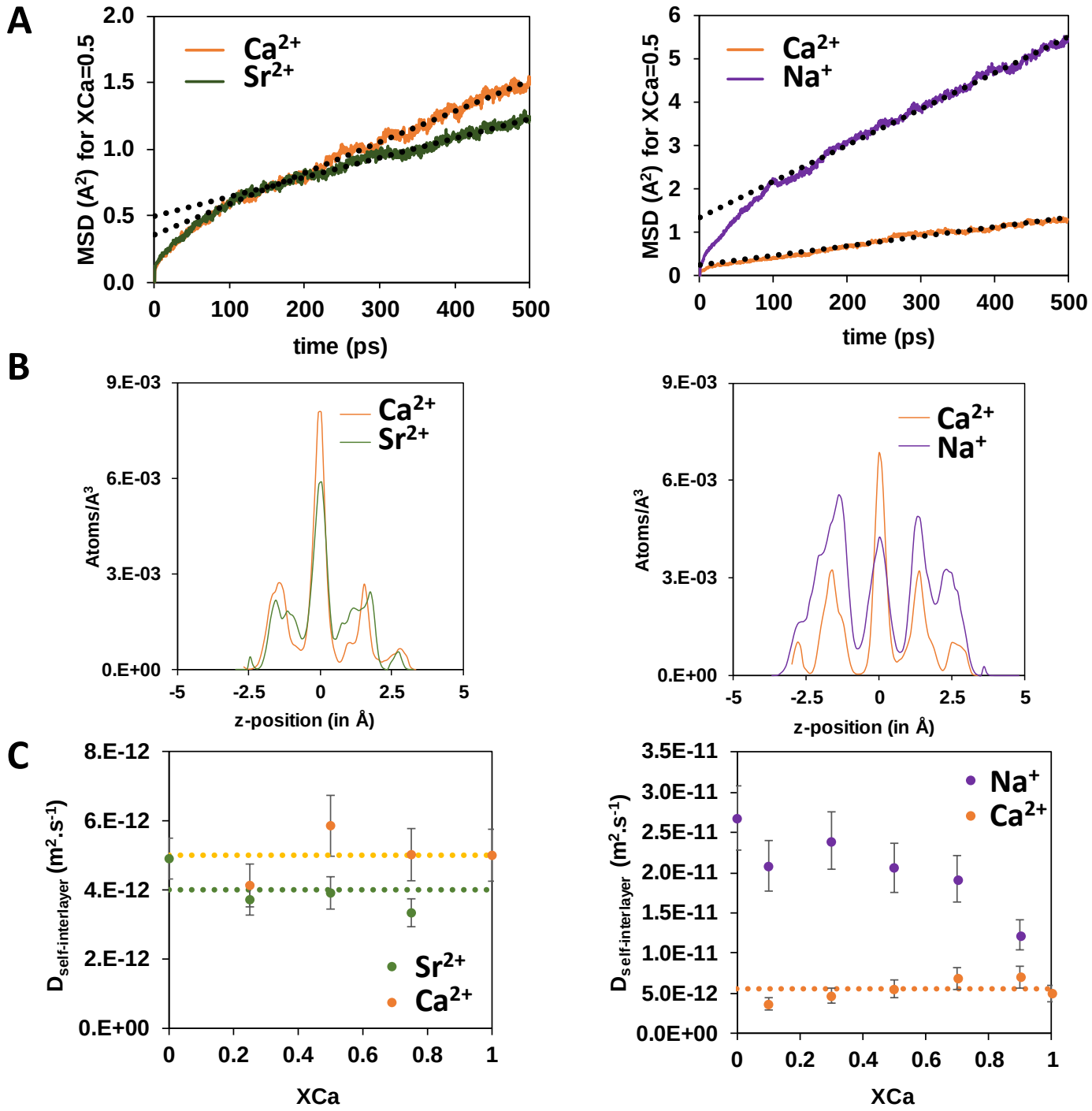
A
MSD (A²) for XCa=0.5
time (ps)
Ca2+
Sr2+
Na+
B
Atoms/A³
z-position (in Å)
C
Dself-interlayer (m².s⁻¹)
XCa

Fig. 2

## A: $Sr^{2+}$-for-$Ca^{2+}$

$D_{self\text{-}interlayer}$ = 4.0±0.6x$10^{-12}$ $m^2.s^{-1}$ (interlayer self-diffusion coefficient of the slowest cation, i.e. $Sr^{2+}$)

–

log $K_c(Sr^{2+}/Ca^{2+})$ = 0

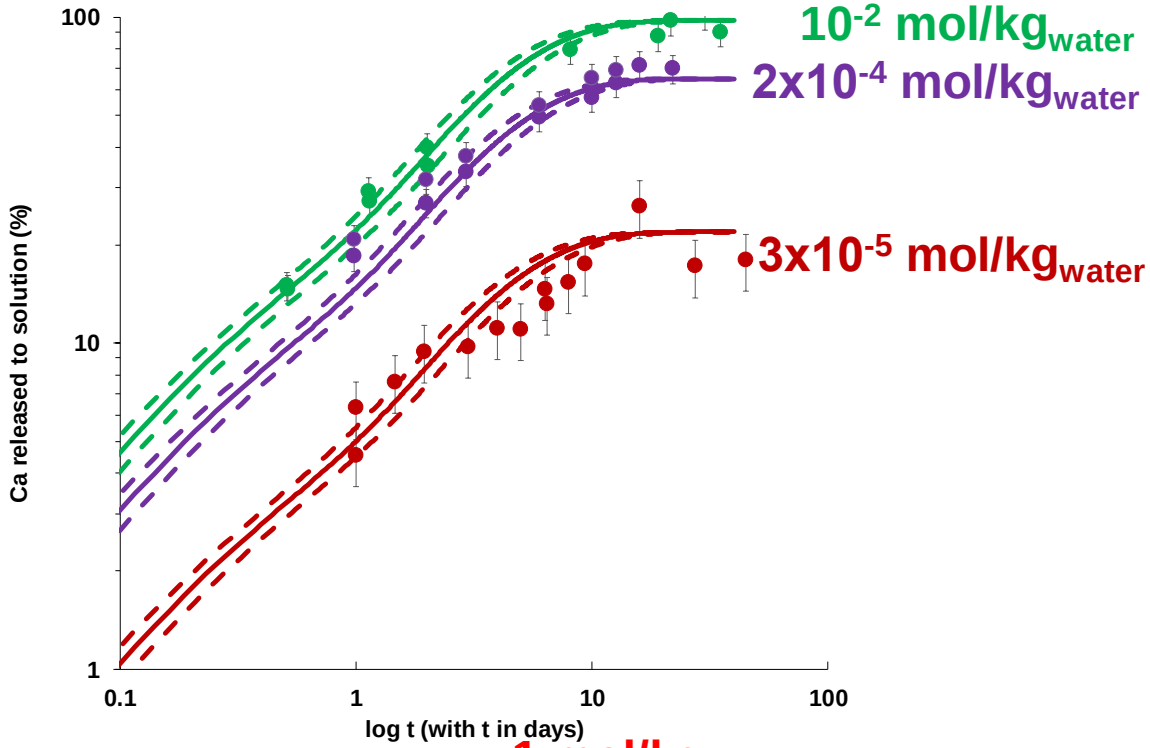


## B: $Na^{+}$-for-$Ca^{2+}$

$D_{self\text{-}interlayer}$ = 5.5±1.9x$10^{-12}$ $m^2.s^{-1}$ (interlayer self-diffusion coefficient of the slowest cation, i.e. $Ca^{2+}$)

–

log $K_c(Na^{+}/Ca^{2+})$ = 0.1

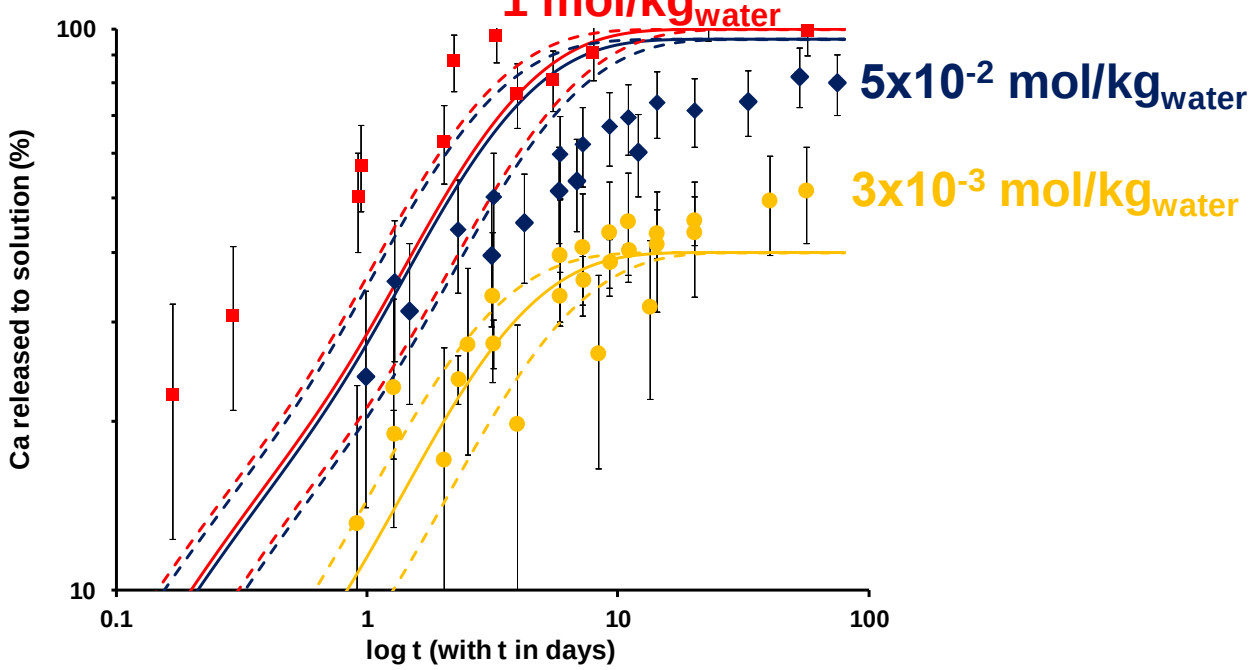

**Fig. 3**

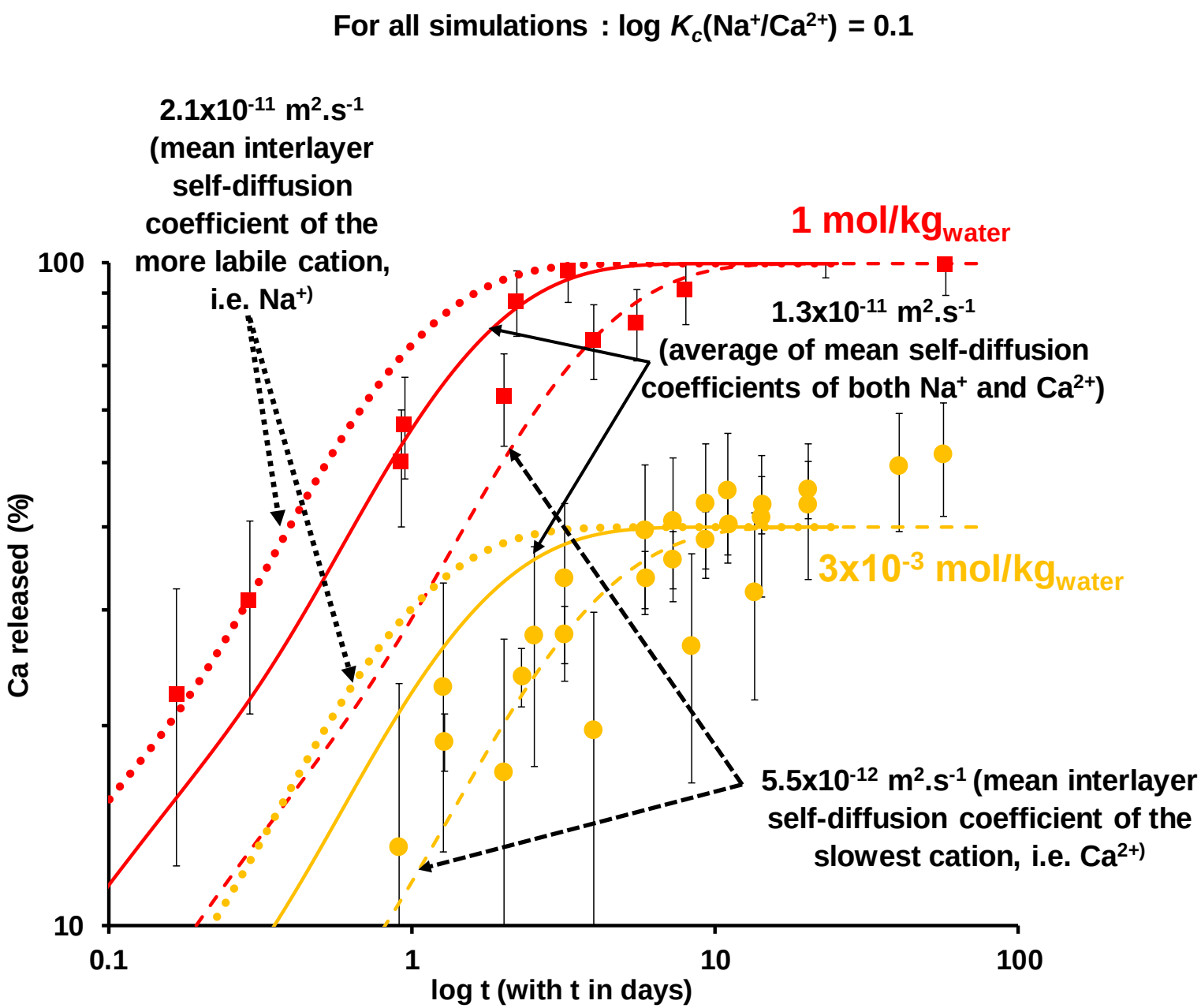
For all simulations : log $K_c(Na^+/Ca^{2+})$ = 0.1
$2.1x10^{-11}$ $m^2.s^{-1}$ (mean interlayer self-diffusion coefficient of the more labile cation, i.e. $Na^{+)}$
1 $mol/kg_{water}$
$1.3x10^{-11}$ $m^2.s^{-1}$ (average of mean self-diffusion coefficients of both $Na^+$ and $Ca^{2+}$)
$3x10^{-3}$ $mol/kg_{water}$
$5.5x10^{-12}$ $m^2.s^{-1}$ (mean interlayer self-diffusion coefficient of the slowest cation, i.e. $Ca^{2+)}$
Ca released (%)
100
10
0.1
1
10
100
log t (with t in days)

Fig. 4

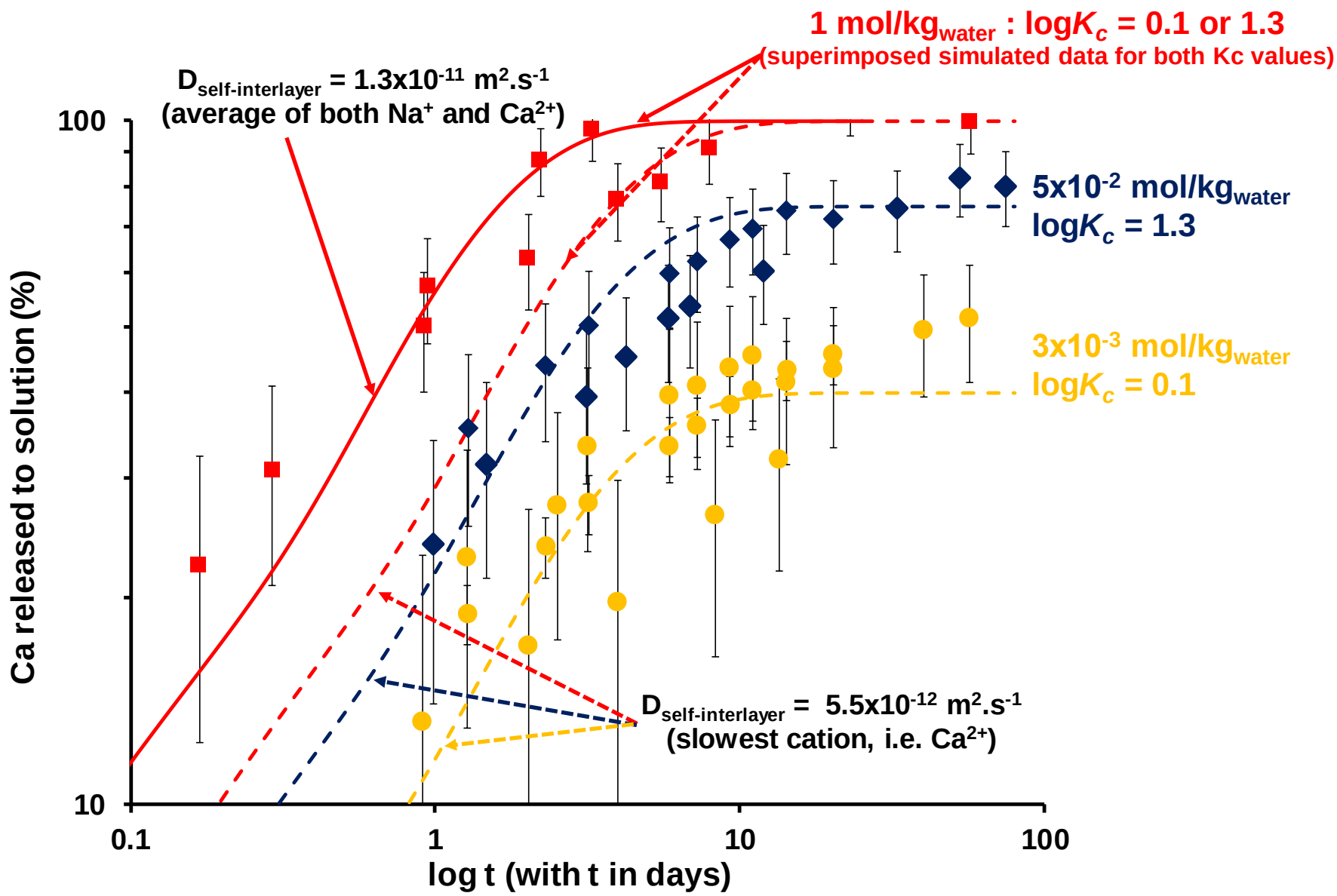
1 mol/kg$_{water}$ : log$K_c$ = 0.1 or 1.3
(superimposed simulated data for both Kc values)
$D_{self\text{-}interlayer}$ = 1.3x10$^{-11}$ m$^2$.s$^{-1}$
(average of both Na$^+$ and Ca$^{2+}$)
5x10$^{-2}$ mol/kg$_{water}$
log$K_c$ = 1.3
3x10$^{-3}$ mol/kg$_{water}$
log$K_c$ = 0.1
$D_{self\text{-}interlayer}$ = 5.5x10$^{-12}$ m$^2$.s$^{-1}$
(slowest cation, i.e. Ca$^{2+}$)
Ca released to solution (%)
100
10
0.1
1
10
100
log t (with t in days)

1 Table 1

2

| Ion-exchange reactions | Initial chemical composition of the solution in contact with Ca-disk (concentrations are expressed in mol/$kg_{water}$)[(a)] | Predicted chemical composition of the solution at equilibrium (after ion-exchange reactions) (concentrations are expressed in mol/$kg_{water}$) [(b) and (c)] | % of Ca (normalised to the sample CEC), released in solution, and predicted at infinite time [(see b)] | Amount of initial reactive Ca in the disk ($mmol_{Ca}/g_{hydrated\text{-}solid}$) [(d)] |
|---|---|---|---|---|
| **$Sr^{2+}$-for-$Ca^{2+}$** | $SrCl_2$ $10^{-2}$ | $[Sr^{2+}] = 9.9x10^{-3}$<br>$[Ca^{2+}] = 1.2x10^{-4}$<br>$[Cl^-] = 2.0x10^{-2}$ | 98 | 0.85 |
| | $SrCl_2$ $2x10^{-4}$ | $[Sr^{2+}] = 1.3x10^{-4}$<br>$[Ca^{2+}] = 6.8x10^{-5}$<br>$[Cl^-] = 4.0x10^{-4}$ | 65 | 0.57 |
| | $SrCl_2$ $3x10^{-5}$ | $[Sr^{2+}] = 6.8x10^{-6}$<br>$[Ca^{2+}] = 2.4x10^{-5}$<br>$[Cl^-] = 6.0x10^{-5}$ | 22 | 0.19 |
| **$Na^+$-for-$Ca^{2+}$** | NaCl 1 | $[Na^+] = 1.0x10^{0}$<br>$[Ca^{2+}] = 1.1x10^{-4}$<br>$[Cl^-] = 1.0x10^{0}$ | 100 | 0.88 |
| | NaCl $5x10^{-2}$ | $[Na^+] = 5.0x10^{-2}$<br>$[Ca^{2+}] = 1.0x10^{-4}$<br>$[Cl^-] = 5.0x10^{-2}$ | 97 | 0.85 |
| | NaCl $3x10^{-3}$ | $[Na^+] = 2.9x10^{-3}$<br>$[Ca^{2+}] = 4.1x10^{-5}$<br>$[Cl^-] = 3.0x10^{-3}$ | 39 | 0.34 |

3 [(a)] pH of all initial solutions used are equal to 5.9 ± 0.15

[b] Calculations are performed assuming a thermodynamic equilibrium between initial solution and a mass of hydrated solid equal to 0.12 g for 1 $kg_{water}$. This solid/solution value is representative of experiments using millimeter Ca-disks, and is equivalent to consider a CEC for disk equal to 175 meq/100$g_{hydrated\text{-}solid}$ in agreement with published value for this parameter (Dzene et al., 2016). Calculations are performed using the Phreeqc® software (Parkhurst and Appelo, 1999) and previous models proposed by Dzene et al. (2016) and Tertre et al. (2013) predicting $Sr^{2+}$-for-$Ca^{2+}$and $Ca^{2+}$-for-$Na^{+}$ interlayer exchange respectively in vermiculite. In these models, decimal logarithms of selectivity coefficients for $Sr^{2+}$-for-$Ca^{2+}$and $Ca^{2+}$-for-$Na^{+}$ (Gaines Thomas convention; Gaines and Thomas, 1953) are equal to 0 and 0.1 respectively (see text for details).

[c] predicted pH of the solution after exchange reactions was close to initial one (± 0.1) even by taking into account the possible adsorption of $H^{+}$ in the model. This data show that adsorption of $H^{+}$ during $Sr^{2+}$-for-$Ca^{2+}$and $Na^{+}$-for-$Ca^{2+}$ exchange reactions is negligible at the pH of the experiments performed in this study (i.e., around pH = 6) using millimetre-sized crystals.

[d] Amounts of initial reactive Ca located in the disk at time 0 were calculated by using the % of Ca (normalised to the sample CEC) released in solution and predicted at infinite time, the solid/solution ratio used for the experiment (i.e., 0.12 g/$kg_{water}$) and a CEC equal to 175 meq/100$g_{hydrated\text{-}solid}$ (Dzene et al., 2016).

# Graphical abstract